Supporting Information

Atomic-level Coupled Spinel@perovskite Dual-phase Oxides toward Enhanced Performance in Zn-air Batteries

Jiaqi Ran[a], Jian-Feng Wu[b], Yongfeng Hu[c], Mohsen Shakouri[c], Baorui Xia*[a], Daqiang Gao[a].

[a]Key Laboratory for Magnetism and Magnetic Materials of MOE, Key Laboratory of Special Function Materials and Structure Design of MOE, Lanzhou University, Lanzhou 730000, P. R. China

[b]State Key Laboratory of Applied Organic Chemistry; Key Laboratory of Nonferrous Metals Chemistry and Resources Utilization of Gansu Province; Advanced Catalysis Center; College of Chemistry and Chemical Engineering; Lanzhou University, Lanzhou 730000, People's Republic of China

[c]Canadian Light Source Inc. University of Saskatchewan; Saskatoon; Saskatchewan, S7N2V3, Canada

Liquid Zn-Air Battery Assembly: Conventional Zn-air battery fabricated by Zn plate (anode), 6 M KOH with a 0.2 M zinc acetate (electrolyte solution) and the prepared electrocatalyst ink is dropped onto a carbon fiber paper (air cathode) with a loading amount of 2.0 mg/cm^2.

Solid-type Zn–air battery assembly: the Zn foil (anode) and the carbon fiber paper with catalyst ink (air cathode) inserted into the manufactured PVA glue (electrolyte). The PVA glue fabricated as follows: PVA powder (2 g) was dissolved into distilled water (20 mL) under magnetic stirring for about 2 h (95 °C). Subsequently, 18M KOH solution (2 mL) was added into transparent gel and kept stirring for about 40min (95 °C) Then,the cooled PVA gule transferred to centrifugal tube and the tube was kept in a refrigerator for 8 h. Eventually, the glue is deforsted and ready for electrolyte.

Material characterizations: The XRD patterns were recored on a Philips/X, Pert PRO diffractometer with Cu Kα radiation. The EELS (Apreo S) and XPS (Kratos AXIS Ultra, corrected with C1s line at 284.6 eV) could be employed to analyses the elementary composition of the samples and the bonding characteristics. The SEM and

TEM images of catalysts were collected using Apreo S and Tecnai G2 F30, FEI, respectively. The HRTEM images were obtained by Themis Titan G2 80-300. ESR measurements were performed on a Bruker ER 200D spectrometer at room temperature.

Calculation details

The number of electron transfer per O_2 participate in oxygen reduction can be determined by Koutechy-Levich equation: [1, 2]

$$1/j = 1/j_k + 1/(B\omega^{1/2}) \quad (1)$$

Where j is the measured current on RDE, j_k is the dynamic current density, and ω is the angular velocity of the disk. B is the slope of the Koutechy-Levich (K-L) plots calculated by the Levich equation below:

$$B = 0.2nF(D_{O_2})^{2/3}v^{-1/6}C_{O_2} \quad (2)$$

Where n stand for the number of transferred electrons per oxygen molecule. F stand for Faraday constant (F = 96485 C/mol). D_{O_2} stand for the diffusion coefficient of Oxygen in 0.1 M KOH (D_{O_2}= 1.9×10^{-5} cm^2/s). v stand for the motion viscosity (v = 0.01 cm^2/s) in the electrolyte solution. C_{O_2} stand for the bulk concentration of O_2 (C_{O_2} = 1.2×10^{-6} mol/cm^3).

The specific capacity was calculated by the equation below: [3]

$$\eta = a + b \times \log j \quad (3)$$

Where η stand for the overpotential, b stands for the Tafel slope, j stands for the current density.

The calculation of overpotential for OER: [4]

$$\eta = E_{RHE} - 1.23 \tag{4}$$

Calculated electrochemical active surface area

$$A_{ECSA}^{LaCoO3} = \frac{6.4 \times 1000\ \mu F\ cm^{-2}}{40\ \mu F\ cm^{-2}\ per\ cm_{ECSA}^{2}} = 160\ cm_{ECSA}^{2} \tag{5}$$

$$A_{ECSA}^{Co3O4@LaCoO3} = \frac{10.5 \times 1000\ \mu F\ cm^{-2}}{40\ \mu F\ cm^{-2}\ per\ cm_{ECSA}^{2}} = 262.5\ cm_{ECSA}^{2} \tag{6}$$

$$A_{ECSA}^{Co3O4} = \frac{8.5 \times 1000\ \mu F\ cm^{-2}}{40\ \mu F\ cm^{-2}\ per\ cm_{ECSA}^{2}} = 212.5\ cm_{ECSA}^{2} \tag{7}$$

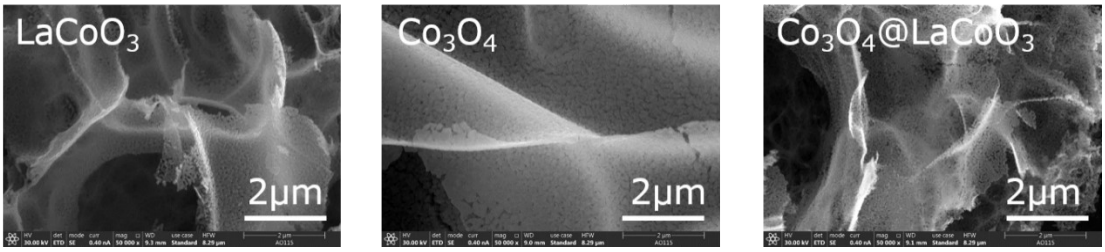

Fig. S1 The scanning electron microscopy (SEM) images of $LaCoO_3$, Co_3O_4 and Co_3O_4@$LaCoO_3$.

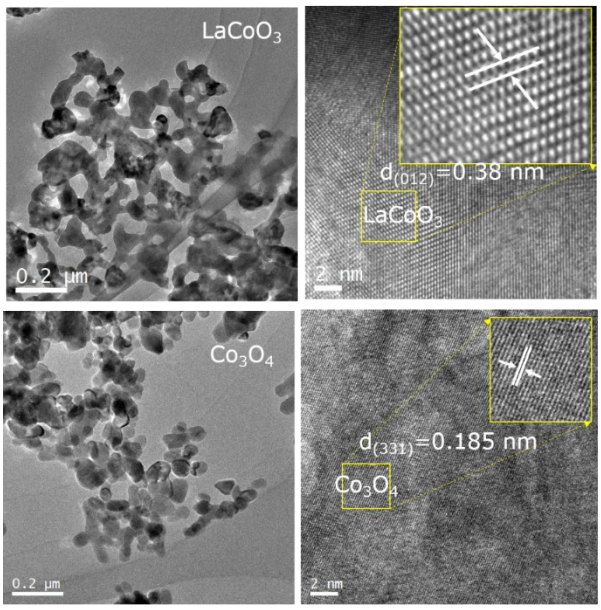

Fig. S2 The TEM and HRTEM images of $LaCoO_3$ and Co_3O_4.

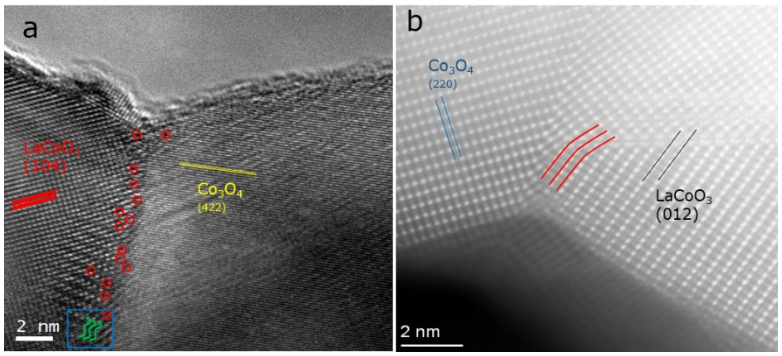

Fig. S3 (a) The HRTEM images and (b) HAADF-STEM image of Co_3O_4@$LaCoO_3$

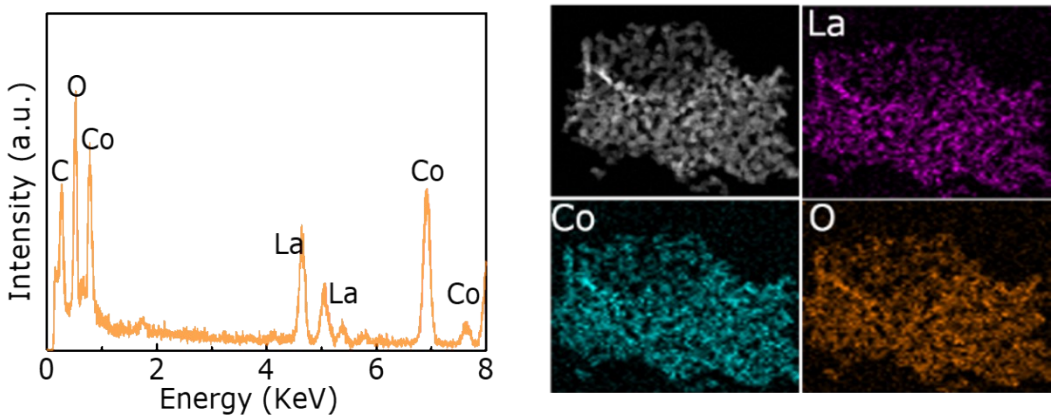

Fig. S4 The HAADF-STEM image and EDS mapping of Co_3O_4@$LaCoO_3$.

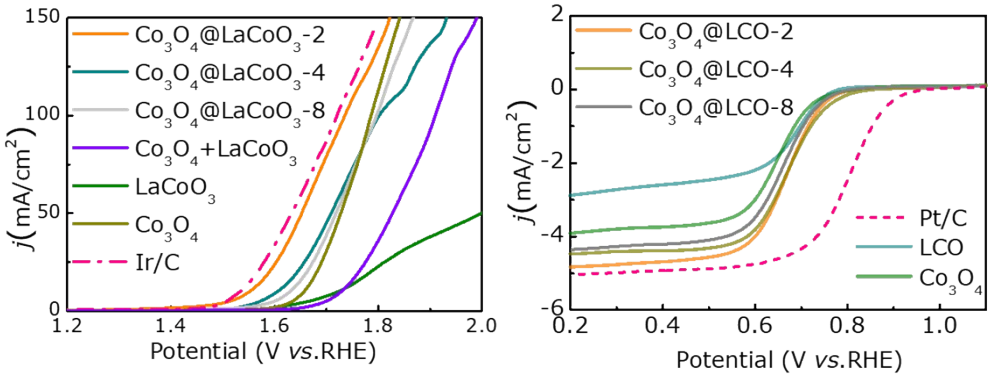

Fig. S5 The OER and ORR polarization curves of all samples.

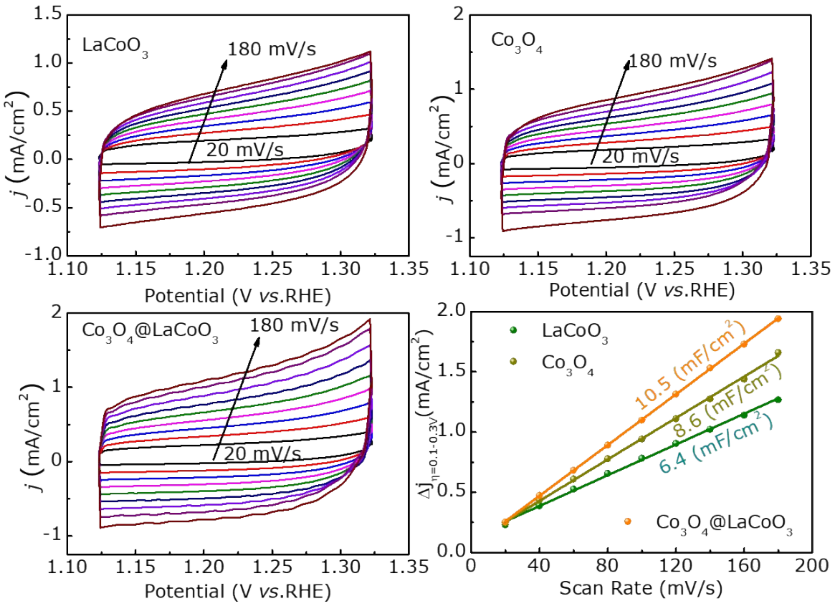

Fig. S6 The cyclic voltammetry curves and the calculated C_{dl} in 1M KOH.

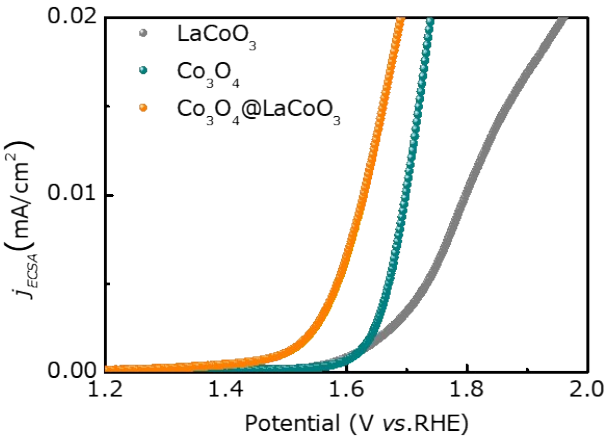

Fig. S7 Polarization curves normalized based on their ECSA.

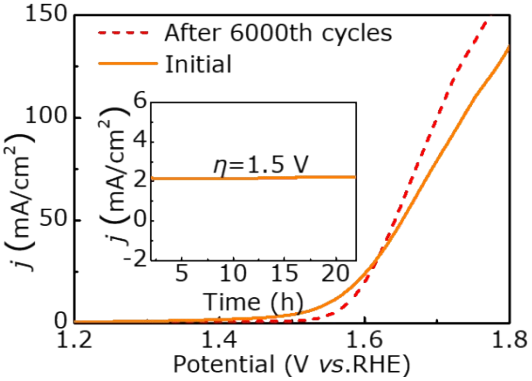

Fig. S8 Curves of Co_3O_4@$LaCoO_3$ after (red line) 6000th cycles and initial (orange line). The inset is the long-term stability test at 1.5 V (versus RHE) for Co_3O_4@$LaCoO_3$.

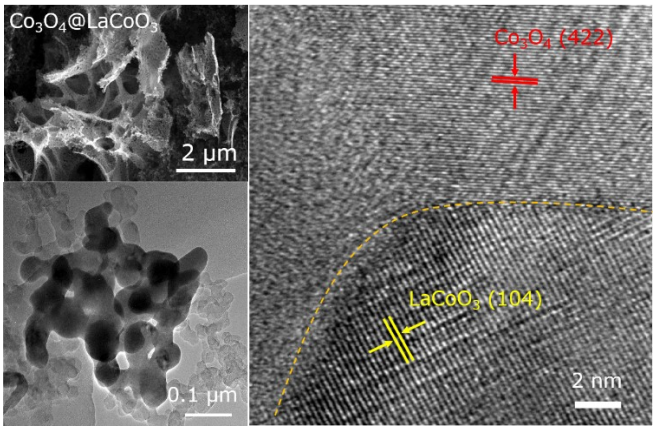

Fig. S9 The SEM, TEM and HRTEM images of Co_3O_4@$LaCoO_3$ after OER stability test.

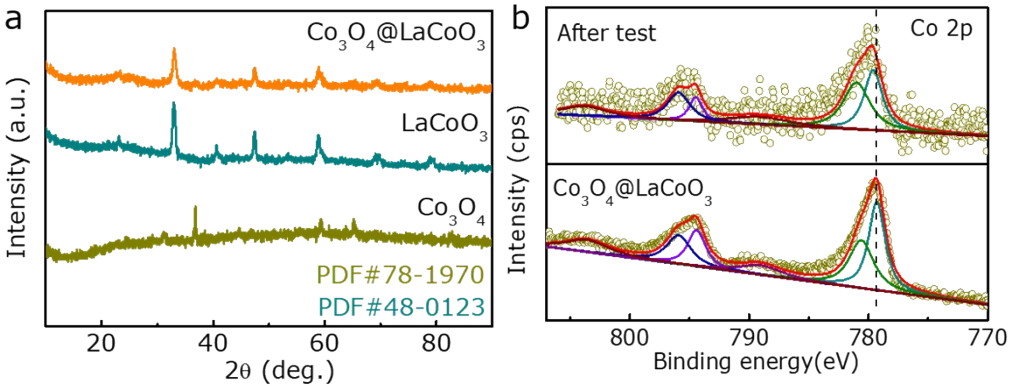

Fig. S10 (a) The XRD patterns and (b) Co 2p XPS spectrum of Co_3O_4@$LaCoO_3$ after OER stability test.

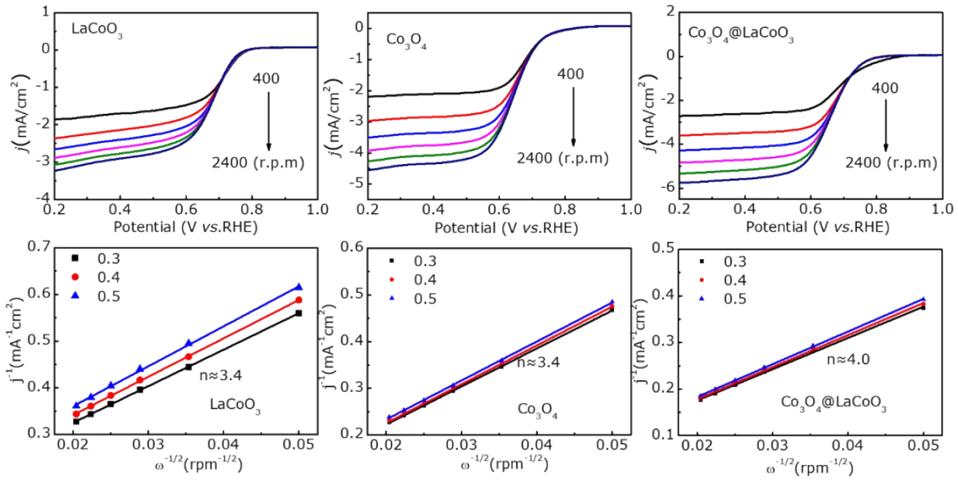

Fig. S11 Different rotating speeds from 400 to 2400 rmp for ORR polarization curves and K-L plots of $LaCoO_3$, Co_3O_4 and Co_3O_4@$LaCoO_3$.

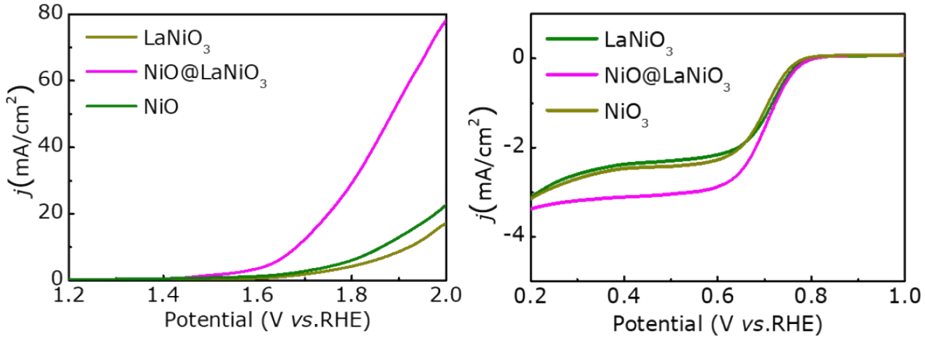

Fig. S12 The OER and ORR polarization curves of $LaNiO_3$, NiO@$LaNiO_3$, NiO.

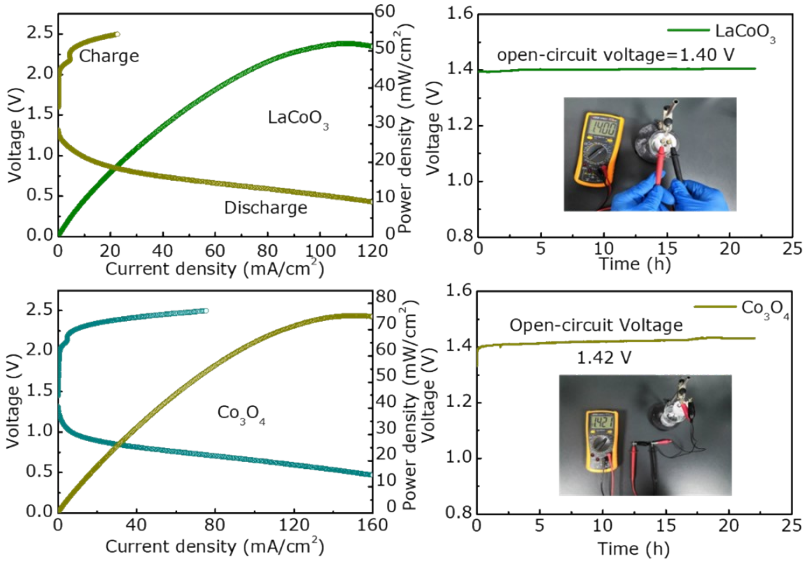

Fig. S13 The power density curve and the open-circuit voltage of $LaCoO_3$ and Co_3O_4.

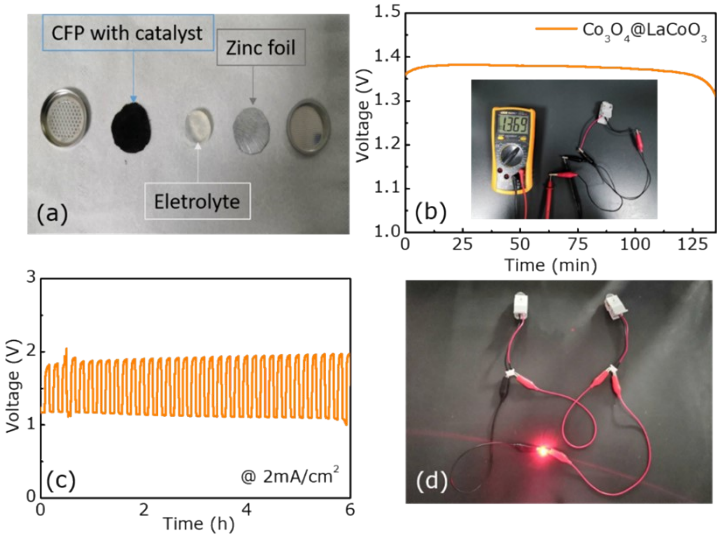

Fig. S14 (a) Structure diagram of solid-button Zn–air battery. (b) The open-circuit curve of the solid-button Zn–air battery. (c) The curves of discharge/charge cycles of the solid-button Zn–air battery under 2 mA/cm^2. (d) The red LEDs powered by two solid-button Zn–air batteries.

Table S1. Comparison of the electrocatalytic activities of Co_3O_4@$LaCoO_3$ with some representative Co-based OER electrocatalysts reported in 1.0 M KOH solution.

catalysts	$E_{j=10\ mA/cm2}$ (mV)	Ref.
Co_3O_4@$LaCoO_3$	320	This work
$LaCoO_3$	490	This work
Co_3O_4	430	This work
Co_9S_8@MoS_2	342	[5]
Co@Co_3O_4-Gr	430	[6]
CoS-$Co(OH)_2$@MoS_{2+x}-NF	380	[7]
CoNC@MoS_2/CNF	350	[8]
CoO/Mn_3O_4	455	[9]
MnO/PAC	421	[10]

Table S2. Performances of recently reported liquid Zn-air batteries.

Catalysts	Power density (mW/cm^2)	Specific capacity (mAh/g_{Zn})	Ref.
Co_3O_4@$LaCoO_3$	140	785	This work
$Fe_{0.5}Co_{0.5}O_x$/NrGO	86	756	[11]
$NiCo_2S_4$@g-C_3N_4-CNT	142	485.7	[12]
$Co_3FeS_{1.5}(OH)_6$	113	843	[13]
NiO/CoN PINWs	80	690	[14]
Pt/C||RuO_2	150	768	[10]

References

(1) Y. Fu, H. Y. Yu, C. Jiang, T. H. Zhang, R. Zhan, X. W. Li, J. F. Li, J. H. Tian and R. Z. Yang, *Adv. Funct. Mater*. *2018*, **28**, 1705094.

(2) L. Ma, S. Chen, Z. Pei, Y. Huang, G. Liang, F. Mo, Q. Yang, J. Su, Y. H. Gao, J. Zapien, and C. Zhi, *ACS Nano 2018*, **12**, 1949.

(3) A. C. Thenuwara, E. B. Cerkez, S. L. Shumlas, N. H. Attanayake, I. G. McKendry, L. Frazer, E. Borguet, Q. Kang, R. C. Remsing and M. L. Klein, *Angew. Chem. Int. Ed. 2016*, **55**, 10381.

(4) P. Liu, J. Ran, B. Xia, S. Xi, D. Gao and J. Wang, *Nano-Micro Lett. 2020*, **12**, 68.

(5) J. Bai, T. Meng, D. Guo, S. Wang, B. Mao and M. Cao, *ACS Appl. Mater. Interfaces 2018*, **10**, 1678–1689.

(6) M. M. Islam, S. N. Faisal, T. Akhter, A. K. Roy, A. I. Minett, K. Konstantinov and S. X. Dou, *Part. Part. Syst. Charact. 2017*, **34**, 1600386.

(7) T. Yoon and K. S. Kim, *Adv. Funct. Mater. 2016*, **26**, 7386-7393.

(8) D. Ji, S. Peng, L. Fan, L. Li, X. Qin and S. Ramakrishna, *J. Mater. Chem. A 2017*, **5**, 23898-23908.

(9) C. Guo, Y. Zheng, J. Ran, F. Xie, M. Jaroniec and S. Z. Qiao, *Angew. Chem. Int. Ed. 2017*, **56**, 8539.

(10) X. F. Lu, Y. Chen, S. Wang, S. Gao and X. W. Lou (David), *Adv. Mater. 2019*, **31**, 1902339.

(11) L. Wei, H. E. Karahan, S. L. Zhai, H. W. Liu, X. C. Chen, Z. Zhou, Y. J. Lei, Z. W. Liu and Y. Chen, *Adv. Mater. 2017*, **29**, 1701410.

(12) X. Han, W. Zhang, X. Ma, C. Zhong, N. Zhao, W. Hu and Y. Deng, *Adv. Mater. 2019*, **31**, 1808281.

(13) H. F. Wang, C. Tang, B. Wang, B. Q. Li and Q. Zhang, *Adv. Mater. 2017*, **29**, 1702327.

(14) J. Yin, Y. X. Li, F. Lv, Q. H. Fan, Y. Q. Zhao, Q. L. Zhang, W. Wang, F. Y. Cheng, P. X. Xi and S. J. Guo, *ACS Nano 2017*, **11**, 2275.